

Capillary driven flow in oval tubes under microgravity

Cite as: Phys. Fluids **33**, 032111 (2021); <https://doi.org/10.1063/5.0040993>

Submitted: 18 December 2020 • Accepted: 10 February 2021 • Published Online: 18 March 2021

 Shangtong Chen (陈上通), Zhijun Ye (叶致君),  Li Duan (段俐), et al.

COLLECTIONS

 This paper was selected as an Editor's Pick



View Online



Export Citation



CrossMark

ARTICLES YOU MAY BE INTERESTED IN

[Why do anguilliform swimmers perform undulation with wavelengths shorter than their bodylengths?](#)

Phys. Fluids **33**, 031911 (2021); <https://doi.org/10.1063/5.0040473>

[Referee acknowledgment for 2020](#)

Phys. Fluids **33**, 020201 (2021); <https://doi.org/10.1063/5.0043282>

[Shear-dependent microvortices in liquid-liquid flow-focusing geometry: A theoretical, numerical, and experimental study](#)

Phys. Fluids **33**, 032016 (2021); <https://doi.org/10.1063/5.0039179>

APL Machine Learning

Open, quality research for the networking communities

OPEN FOR SUBMISSIONS MAY 2022

LEARN MORE



Capillary driven flow in oval tubes under microgravity

Cite as: Phys. Fluids **33**, 032111 (2021); doi: [10.1063/5.0040993](https://doi.org/10.1063/5.0040993)

Submitted: 18 December 2020 · Accepted: 10 February 2021 ·

Published Online: 18 March 2021






View Online



Export Citation



CrossMark

Shangtong Chen (陈上通),^{1,2}  Zhijun Ye (叶致君),^{1,2} Li Duan (段俐),^{1,2}  and Qi Kang (康琦)^{1,2,a)} 

AFFILIATIONS

¹Key Laboratory of Microgravity, Institute of Mechanics, Chinese Academy of Sciences, Beijing 100190, China

²College of Engineering and Science, University of Chinese Academy of Sciences, Beijing 100049, China

^{a)}Author to whom correspondence should be addressed: kq@imech.ac.cn

ABSTRACT

The capillary driven flow of a liquid in a tube of elliptical cross section under microgravity is studied in this paper. All the factors including the dynamic contact angle between the liquid and the tube wall, the pressure loss caused by convection, the viscous resistance in the tube and the reservoir, and the curved liquid surface in the reservoir are considered. The equation of capillary driven flow in the tube of elliptical cross section is derived. The flow equation can be transformed into an equation that combines external forces on the control body in the tube. In the case of low Ohnesorge (Oh) numbers, the flow behavior is divided into three time domains by using the capillary force as the driving force that balances with the inertial force in the reservoir, the convective pressure loss in the reservoir, and the viscous resistance in the tube in the three domains, respectively. The liquid climbing height in these three sections is proportional to t^2 , t , and \sqrt{t} , respectively. However, in the case of high Oh numbers, the flow is divided into two regions, something which has not been proposed in previous work about capillary driven flow in cylinder tubes. This study is verified by drop tower experiments and numerical simulation with the volume of fluid method.

Published under license by AIP Publishing. <https://doi.org/10.1063/5.0040993>

I. INTRODUCTION

Capillary driven flow, which is defined here as a spontaneous interfacial flow driven by surface tension force, is a significant part of liquid behavior in spacecraft tanks. In order to control the space liquid effectively, it is necessary to develop theories of capillary driven flow.

Lucas and Washburn¹ first described the dynamic process involved in capillary rise. They verified that the process could be described using a mechanical balance between the capillary, viscous and gravity forces, which resulted in the well-known Lucas–Washburn equation. Concus and Finn² studied the liquid equilibrium interface in a container with internal angles and proposed the famous Concus–Finn condition. Levine *et al.*³ considered capillary force, viscous force, and convective loss precisely and proposed a theory of capillary rise in cylindrical tubes. Stange *et al.*⁴ proposed a more comprehensive model of capillary rise in cylinder tubes, in which the meniscus reorientation, the dynamic contact angle, and the development of capillary flow were considered. The calculation method of dynamic contact was improved by Jiang *et al.*⁵ and was widely accepted. Dreyer *et al.*⁶ used the same method to explore capillary rise

between parallel plates. Weislogel and Lichter⁷ obtained accurate prediction of liquid flow along interior corners, and it was extended to interior corners with varying wettability (Weislogel and Nardin⁸) and rounded interior corners (Chen *et al.*⁹). Higuera *et al.*¹⁰ analyzed the penetration of a wetting liquid in the narrow gap between two vertical plates making a small angle. Wolf *et al.*¹¹ proposed the Lattice–Boltzmann method based on field mediators to simulate the capillary rise process between parallel plates by considering the effect of long-range interactions between the fluids and the solid walls. Bolleddula *et al.*¹² presented a new analytic solution for flows along planar interior edges. A selection of test cell geometries has then been discussed in the case where compound capillary flows occur spontaneously and simultaneously on local and global length scales. Li *et al.*¹³ established the governing equation of capillary driven flow in cylindrical interior corners and obtained the approximate analytical solution. Reyssat¹⁴ explored capillary bridges between a plane and a cylindrical wall and obtained accurate prediction of the bridges' shape. Wu *et al.*¹⁵ established a comprehensive theoretical model to study the capillary flow along curved interior corners. By analysis, the centrifugal force caused

by the curve motion is the decisive factor, which makes the capillary flow in curved interior corners different from that in straight interior corners. Dushin *et al.*¹⁶ investigated the capillary driven filtration in porous media under microgravity conditions. A new mathematical model that allows taking into account the blurring of the front due to the instability of displacement has been proposed. Chassagne *et al.*¹⁷ explored capillary driven infiltration of liquids into porous structures. An analytical approach, as well as computer simulations based on the free surface lattice Boltzmann (FSLB) method were presented. Chen *et al.*¹⁸ used the capillary flow theory to optimize the structure of propellant management device (PMD) in tanks and conducted drop tower experiments and simulation analyses with the volume of fluid (VOF) method to examine its performance.

In this paper, a mathematical model of capillary rise in oval tubes under microgravity is presented. The influences of the dynamic contact angle, the pressure loss, the viscous resistance, and the curved liquid surface in the reservoir on the capillary rise process are all analyzed. The model is verified by drop tower experiments and numerical simulation with the VOF method. Furthermore, the differential equation is transformed into an equation, which is composed of a series of forces. And, the whole process is divided into different parts by equating only two dominant forces at the same time.

II. THEORETICAL ANALYSIS

As Fig. 1 shows, the meniscus height is named h and the meniscus average velocity is \dot{h} . The semi-major axis and semi-minor axis of the oval tube are, respectively, a and b . A horizontal cross section of the oval tube is shown in Fig. 2. The static contact angle and dynamic contact angle of the liquid on the tube is α and α_d , respectively. Owing to liquid imbibition into tubes and the obstruction of anti-climb baffles, there forms a curved meniscus in the reservoir, with a radius named R_c . It is calculated by the distance between the wetting barriers, c , and the radius of the centerline of the free surface inside the reservoir, d .

For convenience, the Cartesian coordinate system is selected to analyze this problem. The basic assumptions for theoretical analysis are listed below:

- No stress acts on the free surface.

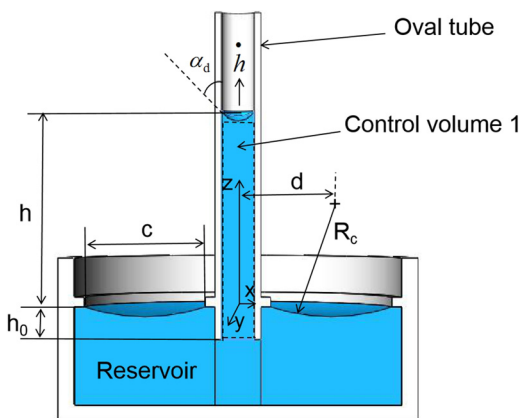


FIG. 1. The front view of the oval tube flow.

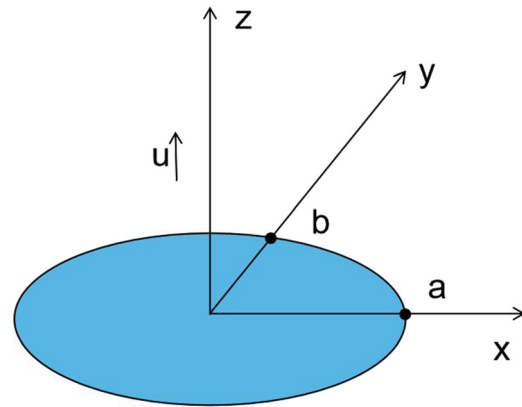


FIG. 2. A horizontal cross section of the oval tube.

- The flowing process is isothermal.
- It is fully developed Poiseuille flow.
- The liquid is Newtonian, incompressible, and homogeneous.
- There is no slip between the flowing liquid and the walls.

From the N-S equation, it is easy to obtain the velocity field in a horizontal cross section of the oval tube

$$u(x, y, t) = 2\dot{h} \left[1 - \left(\frac{x^2}{a^2} + \frac{y^2}{b^2} \right) \right]. \quad (1)$$

From the N-S equation for component u , it yields

$$\frac{\partial u}{\partial t} = -\frac{1}{\rho} \frac{\partial p}{\partial z} + \nu \left(\frac{\partial^2 u}{\partial x^2} + \frac{\partial^2 u}{\partial y^2} \right), \quad (2)$$

where ρ is the liquid density and ν is the kinematic viscosity. Integrating with respect to x and y over the entire horizontal cross section of the oval tube, it can be obtained that

$$\frac{\partial}{\partial t} \iint_{\Omega} u dx dy = \iint_{\Omega} \frac{-1}{\rho} \frac{\partial p}{\partial z} dx dy + \nu \iint_{\Omega} \left(\frac{\partial^2 u}{\partial x^2} + \frac{\partial^2 u}{\partial y^2} \right) dx dy, \quad (3)$$

where Ω represents the entire horizontal cross section of the oval tube. The volume flux across the horizontal section is

$$\pi ab \dot{h} = \iint_{\Omega} u dx dy. \quad (4)$$

By integrating Eq. (3) with respect to z from $z = -h_0$ to $z = h$, we have

$$\begin{aligned} \pi ab (h + h_0) \ddot{h} &= -\frac{1}{\rho} \iint_{\Omega} [p(h, t) - p(-h_0, t)] dx dy \\ &+ \nu \int_{-h_0}^h \iint_{\Omega} \left(\frac{\partial^2 u}{\partial x^2} + \frac{\partial^2 u}{\partial y^2} \right) dx dy dz. \end{aligned} \quad (5)$$

The capillary pressure on the upper control surface is

$$\pi ab p_\sigma = -l\sigma \cos \alpha_d, \tag{6}$$

where l is the approximate circumference of the oval tube's cross section. For a perfectly wetting liquid whose static contact angle is 0, there is an empirical formula for calculating the dynamic contact angle, which is written as

$$\cos \alpha_d = 1 - 2 \tanh \left[4.96 * \left(\frac{\mu v}{\sigma} \right)^{0.702} \right]. \tag{7}$$

where μ is the dynamic viscosity of the liquid, v is its velocity, and σ is its surface tension. This equation was proposed in Ref. 5 and verified by experiments. And, it has been widely accepted. For example, it was adopted to explore capillary rise in cylinder tubes in Ref. 4, as well as to study capillary driven flow between parallel plates in Ref. 6. For convenience, the upper control surface is assumed to be a plane ($x, y, z = h$). The pressure on the upper control surface is

$$p(h, t) = p_0 + p_\sigma, \tag{8}$$

where p_0 is the surrounding air pressure.

To calculate the pressure at the inlet ($x, y, z = -h_0$), a second momentum balance on a control volume in the reservoir is required. The same analysis as in Ref. 3 is used here based on an equivalent circular entrance whose radius, r_e , equals \sqrt{ab} . As shown in Fig. 3, a hemisphere region around the entrance in the reservoir is established and set to be control volume 2 (CV 2). In CV 2, we have

$$I_c = I_e - I_l + \Sigma F, \tag{9}$$

where I_c stands for the rate of change of total momentum in CV 2, I_e represents the flux of momentum entering CV 2, I_l represents the flux of momentum leaving CV 2, and ΣF stands for the sum of forces acting on CV 2.

Combined with the mass conservation equation, the flux of momentum in the z direction entering the hemisphere across $R = r_e$ is

$$2\pi\rho r_e^2 \int_0^{\frac{\pi}{2}} \sin \theta w_{R=r_e}^2 \cos \theta d\theta = \frac{1}{4} \pi \rho r_e^2 \dot{h}^2. \tag{10}$$

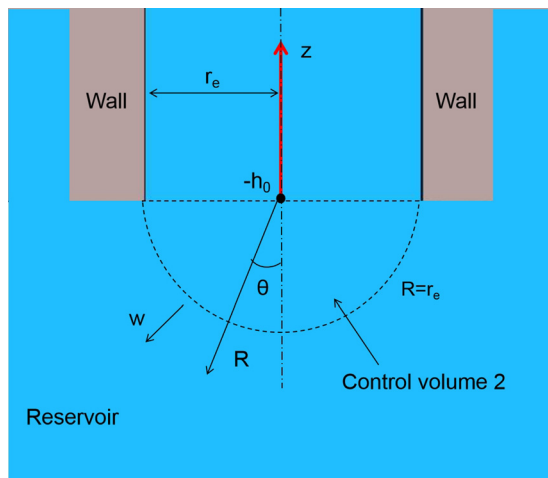


FIG. 3. An equivalent circular entrance and the control volume around the inlet.

The flux of momentum leaving at $z = -h_0$ is

$$\rho \iint_{\Omega} u^2 dx dy = \frac{4}{3} \pi \rho r_e^2 \dot{h}^2. \tag{11}$$

The force in the z direction that exerts over the hemisphere surface $R = r_e$ by the fluid in the reservoir outside $R = r_e$ is

$$x_1 = \pi r_e^2 \left(p_0 + p_R - \frac{1}{2} \rho r_e \ddot{h} - \frac{2\mu}{r_e} \dot{h} \right), \tag{12}$$

where p_R is the capillary pressure caused by R_c . According to the geometric relationship, an approximate equation of R_c can be obtained, which is written

$$R_c = -\frac{c^3 d}{6ab h}, \tag{13}$$

$$p_R = \frac{\sigma}{R_c}. \tag{14}$$

The force in the z direction that exerts over the circular base $z = -h_0$ by the fluid in the equivalent entrance is

$$x_2 = 2\pi \int_0^{r_e} r p(z = -h_0, t) dr. \tag{15}$$

The acceleration distribution inside CV 2 is unknown, so taking the average of acceleration in the volume between the hemisphere surface, $R = r_e$, and the tube entrance, $x, y, z = -h_0$, as the mean acceleration of CV 2, the flux acceleration in the z direction inwards $R = r_e$ is

$$2\pi r_e^2 \int_0^{\frac{\pi}{2}} \left(\frac{Dw}{Dt} \right)_{R=r_e} \sin \theta w_{R=r_e} \cos \theta d\theta = \frac{1}{4} \pi r_e^2 \dot{h} \left(\ddot{h} + \frac{1}{r_e} \dot{h}^2 \right). \tag{16}$$

And, the flux acceleration in the z direction across $z = -h_0$ is

$$\iint_{\Omega} u \frac{du}{dt} dx dy = \frac{4}{3} \pi r_e^2 \dot{h} \ddot{h}. \tag{17}$$

Therefore, the rate of change of total momentum in CV 2 is $\frac{2}{3} \pi r_e^3 \rho \left(\frac{19}{24} \ddot{h} + \frac{1}{8r_e} \dot{h}^2 \right)$.

Inserting Eqs. (10)–(17) into Eq. (9), we can obtain the pressure force at the inlet, which reads

$$x_2 = \pi r_e^2 (p_0 + p_R) - 2\pi \mu r_e \dot{h} - \frac{37}{36} \rho \pi r_e^3 \ddot{h} - \frac{7}{6} \rho \pi r_e^2 \dot{h}^2. \tag{18}$$

Inserting Eqs. (1), (18), and (6)–(8) into Eq. (5), the differential equation for the height of the meniscus can be obtained, written as

$$\ddot{h} = \frac{1}{h + h_0 + \frac{37}{36} r_e} \left\{ \frac{\sigma}{\rho} \left[\frac{l}{\pi ab} \cos \alpha_d - \frac{1}{R_c} \right] - \left[\frac{4(a^2 + b^2)}{(ab)^2} (h + h_0) + \frac{2}{r_e} \right] \nu \dot{h} - \frac{7}{6} \dot{h}^2 \right\}. \tag{19}$$

When a equals b , Eq. (19) becomes the equation for capillary rise in cylinder tubes. Equation (19) can be solved using a fourth-order Runge-Kutta method with the initial conditions, $\dot{h}(t=0) = h(t=0) = 0$. Equation (19) can be scaled using the characteristic

viscous time, $t_c = ab/(8\nu)$, and the characteristic velocity, $v_c = \sqrt{2\sigma/\rho r_e}$. Introducing the dimensionless variables, $t_* = t/t_c$ and $h_* = h/(t_c v_c)$, leads to

$$\ddot{h}_* = \frac{1}{h_* + 8\left(\Lambda_1 + \frac{37}{36}\right)Oh} \left\{ \Lambda_2 \cos \alpha_d - \frac{\Lambda_3 h_*}{16Oh} - [\Lambda_4 h_* + (8\Lambda_1 + 2)Oh] \dot{h}_* - \frac{1}{2} h_*^2 \right\} \quad (20)$$

where $Oh = \mu/\sqrt{\rho\sigma D} = r_e/(8t_c v_c)$, $\Lambda_1 = h_0/r_e$, $\Lambda_2 = l/(2\pi r_e)$, $\Lambda_3 = 6r_e^4/c^3 d$, and $\Lambda_4 = (a^2 + b^2)/(2ab)$. It can be seen that Eq. (20) depends only on the Oh number and the geometric ratios, $\Lambda_1, \Lambda_2, \Lambda_3$, and Λ_4 . This means that Eq. (19) is scaled and non-dimensionalized by using t_c and v_c .

III. DISCUSSION

As Dreyer *et al.* discussed in Ref. 6, Eq. (19) can also be written as a sum of forces. The capillary flow can be divided into different time domains, and in each of them only two forces play the dominant role. With the capillary force in the oval tube being the driving force, Eq. (19) reads

$$F_{ct} = F_{it} + F_{ir} + F_{cr} + F_{ft} + F_{fr} + F_{pl}. \quad (21)$$

The meanings of the force terms are:

- (i) Capillary force in the tube $F_{ct} = l\sigma \cos \alpha_d$.
- (ii) Inertia force in the tube $F_{it} = \rho\pi ab \dot{h}$.
- (iii) Inertia force in the reservoir $F_{ir} = \rho\pi ab \left(\frac{37}{36}r_e + h_0\right) \ddot{h}$.
- (iv) Capillary force in the reservoir $F_{cr} = \frac{6\pi a^2 b^2}{c^3 d} \sigma h$.
- (v) Friction force in the tube $F_{ft} = \frac{4(a^2 + b^2)\pi\mu(h+h_0)}{ab} \dot{h}$.
- (vi) Friction force in the reservoir $F_{fr} = 2\pi\mu r_e \dot{h}$.
- (vii) Pressure loss force at the entrance $F_{pl} = \frac{7}{6}\rho\pi ab \dot{h}^2$.

A typical force progression for SF 1 is shown in Fig. 4, where the x axis is the time, t , and the y axis is the force, F . The red line

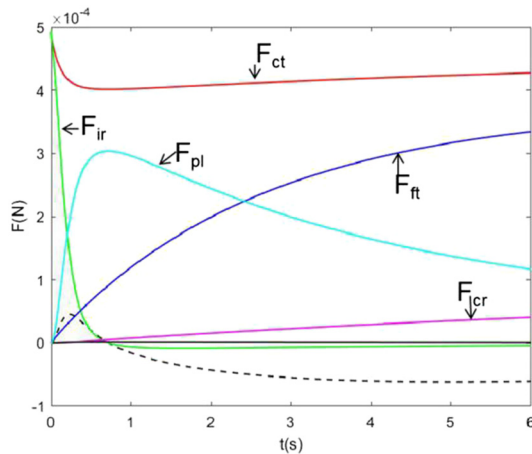


FIG. 4. Development of different forces vs time for Shin-Etsu Silicone Oil KF-96 SF 1 (25 °C) in the oval tube with $a = 5$ mm, $b = 4$ mm, and $h_0 = 20$ mm.

represents the capillary driven force, F_{ct} , the green line stands for the inertia force in the reservoir, F_{ir} , the light blue line represents the pressure loss in the entrance, F_{pl} , the deep blue line represents the friction force in the tube, F_{ft} , the magenta line stands for the capillary force in the reservoir, F_{cr} , and the dashed line stands for the inertia force in the tube, F_{it} . The capillary driven force is effective from the beginning and starts with the maximum value. The initial development of the meniscus from flat to curved equilibrium surface is ignored. As the velocity of the meniscus increases quickly at the beginning, capillary driven force decreases rapidly until it reaches the minimum value. This is due to the influence of dynamic contact angle. Besides the capillary driven force, in the beginning, the inertia force in the reservoir is the dominant force but decreases rapidly. And then, the pressure gradient force plays the dominant role. It reaches its maximum value quickly and decreases with the decreasing velocity of the meniscus. At certain times, the friction force in the oval tube surpasses the pressure gradient force and becomes the major one. Approximate solutions can be obtained by equating only two forces in the respective time domains. The capillary force is always the driving force. Combining the inertia force in the reservoir, F_{ir} , and the capillary force, F_{ct} , in the first time domain, yields the flow speed

$$\dot{h}_1(t) = \frac{F_{ct}}{\pi ab \left(\frac{37}{36}r_e + h_0\right) \rho} t. \quad (22)$$

The initial condition is $\dot{h}(t=0) = 0$. In the second time domain, the capillary force is equated to the pressure gradient force, which yields

$$\dot{h}_2(t) = \sqrt{\frac{6F_{ct}}{7\rho\pi ab}}. \quad (23)$$

Time t_1 in the end of the first time domain can be obtained from the intersection of the two velocity curves, that is

$$t_1 = 1.64r_e \left(\frac{37}{36}r_e + h_0\right) \sqrt{\frac{\rho}{F_{ct}}}. \quad (24)$$

Time t_1 terminates the inertia-controlled domain. To calculate liquid flow velocity in the third region, equating the capillary force with the friction force in the tube. For capillary flow in the case of low Oh number, the initial liquid height, h_0 , can be neglected compared to liquid flow distance in this region

$$\dot{h}_3(t) = \sqrt{\frac{abF_{ct}}{8\pi(a^2 + b^2)\mu}} \frac{1}{\sqrt{t}}. \quad (25)$$

This is a Lucas–Washburn equation for the third time domain. The curves of \dot{h}_2 and \dot{h}_3 intersect at the time, $t_2 = \frac{7a^2b^2}{48(a^2+b^2)\nu} = \frac{7ab}{6(a^2+b^2)} t_c$.

However, the capillary driven flow in oval tubes cannot be divided into three parts in all cases. The development of different forces vs time under different conditions is plotted in Figs. 5 and 6. The meanings of different colored lines are same as those in Fig. 4. Stange *et al.* presented in Ref. 4 that, if Λ_1 was large enough, it was possible to oppress region 2 and the flow changed directly from region 1 into region 3. This rule is also applicable in oval tubes. As Figs. 5(a) and 5(b) show, when Λ_1 equals 8.16, F_{pl} cannot be ignored. But when Λ_1 equals 81.6, F_{pl} can be ignored compared to F_{ir} and F_{ft} , which

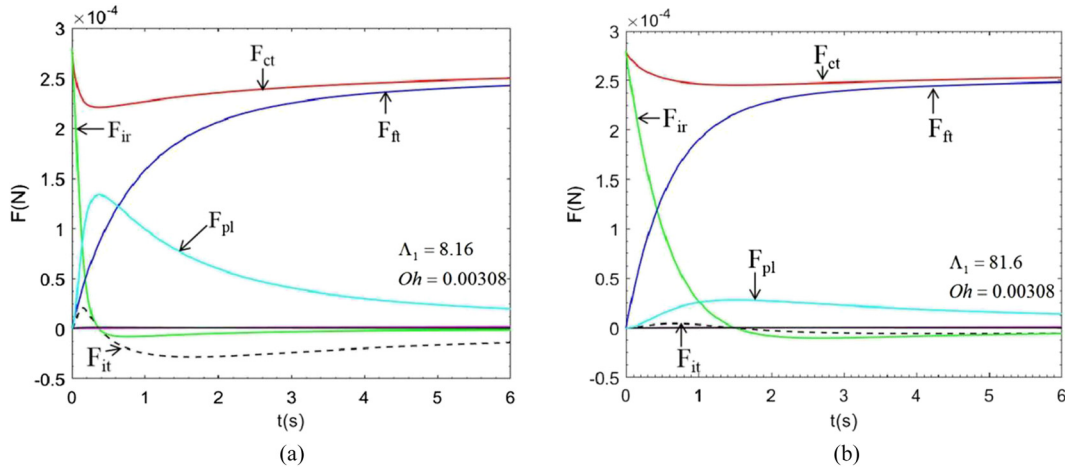


FIG. 5. Development of different forces vs time for SF 1 (25 °C) in the oval tube with $a = 3$ mm, $b = 2$ mm. (a) $h_0 = 20$ mm and (b) $h_0 = 200$ mm.

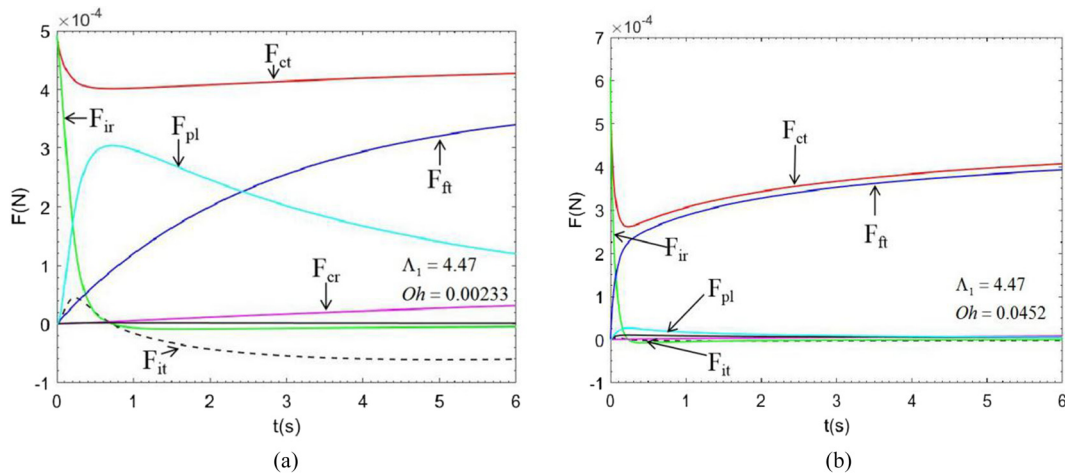


FIG. 6. Development of different forces vs time in the oval tube with $a = 5$ mm, $b = 4$ mm, and $h_0 = 20$ mm. (a) SF 1 (25 °C) and (b) SF 20 (25 °C).

means region 2 does not exist under this condition. They also presented that, in the case of high Oh numbers, regions 1 and 2 were completed very fast. This is not quite accurate according to this study. As presented in Fig. 6(b), the pressure loss force in the entrance, which is used to balance with capillary driven force to calculate velocity in region 2, is much smaller than that in Fig. 6(a), and it can be ignored compared to capillary driven force and friction force in the tube, which means in the case of high Oh number, region 2 is also oppressed. In this condition, the liquid flow speed is not fast and its flow distance is not long enough in the early seconds, so h_0 cannot be ignored. Equating the capillary force with the friction force in the tube, yields

$$h_{2h}(t) = \frac{\sqrt{C_1^2 h_0^2 + 2C_1 F_{ct} t} - C_1 h_0}{C_1} + C, C_1 = \frac{4(a^2 + b^2)\pi\mu}{ab}, \quad (26)$$

where C is a constant. The velocity in the second region becomes

$$\dot{h}_{2h} = \frac{F_{ct}}{\sqrt{C_1^2 h_0^2 + 2C_1 F_{ct} t}}. \quad (27)$$

The moment, t_{1h} , which demarcates these two regions can be obtained by equating \dot{h}_1 and \dot{h}_{2h}

$$t_{1h} = s_1 + s_2, \quad s_1 = \sqrt[3]{\sqrt{\frac{q^2}{4} + \frac{p^3}{27}} - \frac{q}{2}}, \quad s_2 = \sqrt[3]{-\sqrt{\frac{q^2}{4} + \frac{p^3}{27}} - \frac{q}{2}},$$

$$p = -\frac{C_1^2 h_0^4}{12F_{ct}^2}, \quad q = \frac{C_1^3 h_0^6}{108F_{ct}^3} - \frac{C_2^2}{2C_1 F_{ct}}, \quad C_2 = \pi ab \left(\frac{37}{36} r_e + h_0 \right) \rho. \quad (28)$$

In the case of low Oh numbers, from the equations of velocities in different time domains, an approximate solution for $h(t)$ can be obtained. The height before t_1 is

$$h_1(t) = \frac{F_{ct}}{2\pi ab \left(\frac{37}{36}r_e + h_0\right)\rho} t^2 \quad (29)$$

with the initial condition, $h_1(0) = 0$. The height at $t = t_1$ is

$$h_1(t_1) = 0.429 \left(\frac{37}{36}r_e + h_0\right). \quad (30)$$

In the second time domain, the height is

$$h_2(t) = \sqrt{\frac{6F_{ct}}{7\pi\rho ab}}(t - t_1) + h_1(t_1). \quad (31)$$

It can be seen that it is a linear relation between the meniscus height and time. The height at $t = t_2$ is

$$h_2(t_2) = 0.0762 \frac{r_e^3}{(a^2 + b^2)\nu} \sqrt{\frac{F_{ct}}{\rho}} - 0.429 \left(\frac{37}{36}r_e + h_0\right). \quad (32)$$

The third time domain, in which $h_3(t)$ is proportional to \sqrt{t} , is named Washburn domain

$$h_3(t) = \sqrt{\frac{abF_{ct}}{8(a^2 + b^2)\pi\mu}}(\sqrt{t} - \sqrt{t_2}) + h_2(t_2). \quad (33)$$

Therefore, the capillary driven flow in oval tubes is divided into three regions when the Oh number is low and is divided into two regions when the Oh number is high, as shown in Figs. 7(a) and 7(b), where the x axis is time, t , and the y axis is the liquid climbing height, h . The blue line represents the development of height vs time. Different regions are also labeled in the diagrams. In Fig. 7(a), during the first region, the height increases in proportion with t^2 ; during the second region, the height is proportional to t ; and during the Washburn domain, the height is proportional to \sqrt{t} . In Fig. 7(b), during the first region, the height increases in proportion with t^2 ; during the second region, when the liquid flow distance is so long that h_0 can be ignored, the height is also proportional to \sqrt{t} according to Eq. (26).

However, Eqs. (29)–(33) are obtained by simplifying forces, which means that the result is not the exact solution. But, it is quite simple and useful to calculate the transition times and flow distances roughly without solving the exact solution numerically.

IV. COMPARISON BETWEEN THEORETICAL, NUMERICAL, AND EXPERIMENTAL RESULTS

The microgravity experiments are carried out in Beijing Drop Tower. The image acquisition devices can take 50 frames per second. During experiments, the platform is fixed in the drop cabin. It falls freely for 3.5 s first from the top of the drop tower and its microgravity level is 0.001 g. Cylindrical containers made of PMMA with internal diameters of 160 and 100 mm are used for the experiments. The oval tubes, open on top and bottom, are immersed into the liquid from above, as Fig. 1 shows. The measuring devices are attached to the outer sides of tubes to evaluate the flow distance. Wetting barriers are also included in the model. When the velocity field in a horizontal cross section of the oval tube can be expressed by Eq. (1), the capillary driven flow is considered to be fully developed. In order that the flow enters the fully developed stage faster, tubes with small inner sizes are chosen. Generally speaking, when $\nu t/r_e^2 = 0.75$, the flow is considered to be fully developed. For example, when in a tube with $a = 5$ mm and $b = 4$ mm, and SF 10 is used, it will take 1.5 s to get into the fully developed stage. For capillary driven flow in cylinder tubes, there exists a relation for correcting pressure drop, F_{pl} , owing to liquid development at the beginning. The effect of this term is small and the influence caused by absence of this term's correction is negligible as long as liquid enters the fully developed stage quickly.

Several kinds of Shin-Etsu Silicone Oil KF-96, which are labeled by their kinematic viscosity (SF 1, SF 2, SF 10, and SF 20), are used. Their properties are listed in Table I. According to the user manual of Shin-Etsu Company, there exists a relationship between liquid kinetic viscosity and temperature

$$\log_{10}(\nu_T) = \frac{763.1}{273 + T} - 2.559 + \log_{10}(\nu_{25^\circ C}), \quad (34)$$

$$- 25^\circ C \leq T^\circ C \leq 250^\circ C.$$

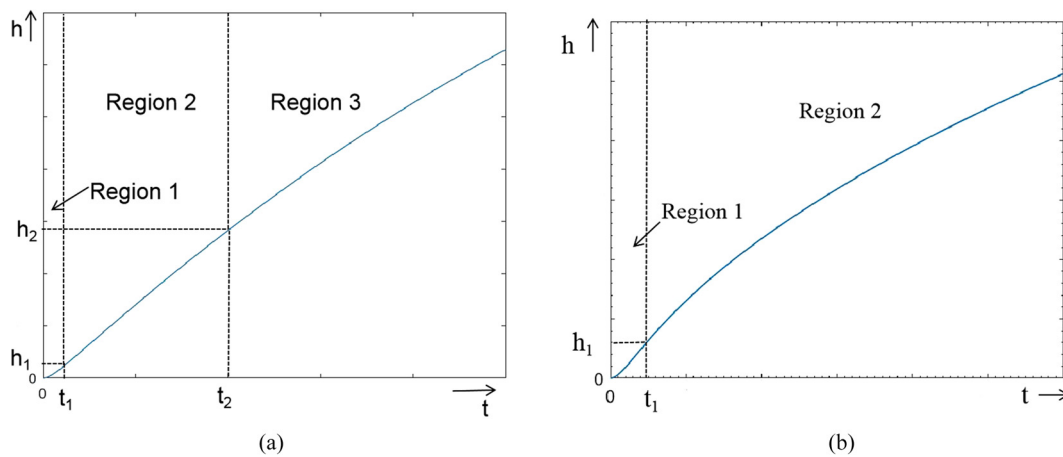


FIG. 7. General representation of capillary rise in oval tubes under microgravity. The meniscus height h vs time t . (a) Capillary driven flow in the case of low Oh numbers, and (b) in the case of high Oh numbers.

TABLE I. Liquid properties.

Liquid	μ [kg/(ms)]	ρ (kg/m ³)	σ (N/m)	ν (mm ² /s)
SF 1 (12.4 °C)	0.001 082	830	0.017 9	1.30
SF 1 (25 °C)	0.000 818	818	0.016 9	1
SF 2 (12.3 °C)	0.002 308	886	0.019 2	2.61
SF 2 (25 °C)	0.001 746	873	0.018 3	2
SF 10 (6.8 °C)	0.014 032	952	0.021 2	14.7
SF 10 (13.0 °C)	0.012 170	946	0.020 8	12.9
SF 10 (25 °C)	0.009 35	935	0.020 1	10
SF 20 (25 °C)	0.019	950	0.020 8	20

Besides, liquid density and surface tension can also be expressed as a function of temperature. For example, for SF 2, its change rate of surface tension with respect to temperature is 7×10^{-5} N/(m K). And its density at a certain temperature is

$$\rho_T = 873 * (1.029 - 0.00116 * T), 0^\circ\text{C} \leq T^\circ\text{C} \leq 25^\circ\text{C}. \quad (35)$$

To ensure the accuracy of the comparison, theoretical calculations and corresponding numerical simulations are performed using the liquid properties at the temperature, which is measured during the respective experiment.

Figure 8 shows a series of frames of capillary rise in a drop tower experiment. The first picture ($t = 0$) shows the liquid surface in the reservoir before the cabin is released. It can be seen that the liquid surface is almost flat and there is no liquid climbing upwards in the tube. The next five pictures present that, once the cabin is released, the reorientation of the liquid surface begins, and the liquid flows into the oval tube. The position of liquid–gas interface in the tube goes higher and higher with time. The climbing height, h , is measured from the video recording frame by frame. For convenience, it is measured every 0.1 s. Figure 8 also shows that a curved free surface is formed in the tube, which is the source of capillary driven pressure.

Corresponding numerical simulation is conducted with the VOF method in Fluent. A typical 3D mesh model is shown in Fig. 9. For convenience, a square-shaped reservoir is used instead of a cylinder-shaped one and its equivalent radius is used in theoretical calculations. Since the effects of capillary force in the reservoir are quite small, the impact of this simplification is negligible. The total number of grids is about 1.2×10^6 . Boundary layers are also established near the walls. The height of the first boundary layer is about 0.1 mm, and the expansion rate between two adjacent layers is 1.2. Each simulation is performed for a second time after the boundary layers are adjusted slightly, and the average is taken as the final result.

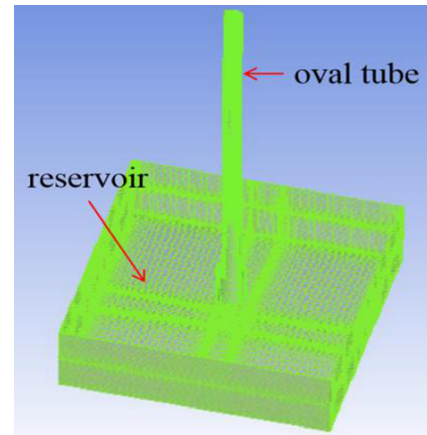


FIG. 9. 3D Mesh model of numerical simulation.

According to Table II, Re number is much smaller than 2000, so the laminar flow is chosen as the flow mode in the simulation. The pressure–velocity coupling equation is numerically solved by SIMPLEC algorithm. The SIMPLEC algorithm uses a relationship between velocity and pressure corrections to enforce mass conservation and to obtain the pressure field. PRESTO is used for the spatially discretized pressure equation. The spatially discretized gradient equation is based on least square cell. The spatially discretized momentum equation uses the second-order upwind style, and Geo-Reconstruct is used for the spatially discretized volume fraction equation. When the iterative residual decreases to 10^{-6} , the calculation is considered to be converged. The relaxation factor for each equation is set by default. During calculations, the Courant number is mostly smaller than 1, which indicates that the calculation process is quite stable. The Courant number is significant for transient flow. For a one-dimensional grid, it is defined by

$$Courant = u\Delta t/\Delta x, \quad (36)$$

where u is the liquid flow speed, Δx is the mesh length and Δt is the time step size. Different time step sizes are adopted for different liquids. The time step size is 0.000 1 s for SF 1, 0.000 2 s for SF 2, 0.000 4 s for SF 10 and 0.000 5 s for SF 20. For comparison, the front position of the meniscus is also recorded every 0.1 s. The numerical result of capillary driven flow is shown in Fig. 10. The red part represents the liquid. The entire height of the model is 170 mm. At the beginning, the liquid is all in the bottom. As soon as the simulation begins, it flows upwards quickly into the oval tube and forms a concave surface in the tube.

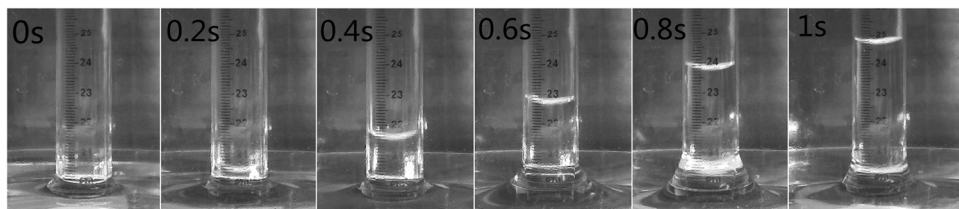


FIG. 8. Capillary rise of SF 2 (12.3 °C) in an oval tube with $a = 7$ mm, $b = 4$ mm, and $h_0 = 12$ mm.

TABLE II. Experimental and numerical parameters.

No.	a (mm)	b (mm)	h_0 (mm)	Liquid	v_{\max} (mm/s)	Re_{\max}	t_c (s)	v_c (mm/s)	t_1/t_{1h} (s)	t_2 (s)	$Oh \cdot 10^{-3}$	Experimental or numerical
#1	3	2	15	SF 1 (25 °C)	90.5	443	0.750	129.9	0.134	0.404	3.08	Numerical
#2	3	2	15	SF 10 (25 °C)	32.1	44.3	0.075	132.5	0.106	...	30.8	Numerical
#3	5	4	10	SF 10 (6.8 °C)	29.6	18.0	0.170	99.8	0.154	...	33.0	Both
#4	5	4	10	SF 10 (13.0 °C)	31.9	22.2	0.194	99.2	0.154	...	29.0	Both
#5	5	4	20	SF 1 (25 °C)	71.4	639	2.50	96.1	0.255	1.42	2.33	Numerical
#6	5	4	20	SF 1 (12.4 °C)	70.1	481	1.92	98.0	0.171	1.09	2.97	Both
#7	5	4	20	SF 20 (25 °C)	19.6	8.76	0.125	97.3	0.215	...	45.2	Numerical
#8	6	3	15	SF 1 (25 °C)	74.9	636	2.25	98.7	0.186	1.05	2.40	Numerical
#9	6	3	15	SF 2 (25 °C)	65.4	277	1.13	99.4	0.191	0.525	4.70	Numerical
#10	6	3	15	SF 10 (25 °C)	33.1	28.1	0.225	101	0.167	...	23.4	Numerical
#11	6	5	15	SF 1 (25 °C)	66.5	728	3.75	86.9	0.238	2.15	2.10	Numerical
#12	6	5	15	SF 2 (25 °C)	59.7	327	1.88	87.5	0.246	1.08	4.2	Numerical
#13	6	5	15	SF 10 (25 °C)	34.0	37.2	0.375	88.6	0.251	...	20.6	Numerical
#14	7	4	12	SF 2 (12.3 °C)	58.5	238	1.34	90.5	0.197	0.675	5.44	Both
#15	7	4	12	SF 1 (25 °C)	69.3	733	3.50	88.4	0.190	1.76	2.10	Numerical
#16	7	4	12	SF 2 (25 °C)	62.2	329	1.75	89.0	0.197	0.880	4.20	Numerical
#17	7	4	12	SF 10(25 °C)	35.3	37.4	0.35	90.1	0.201	...	21.0	Numerical

Figures 11(a) and 11(b) present the comparison between theoretical and numerical results. In the figures, the curves represent the theoretical height vs time, and the square signs stand for numerical results. It can be seen that the numerical results are in good agreement with theoretical ones. According to Table II, the moments that demarcate different regions are labeled in Figs. 11(a) and 11(b). In Fig. 11(a), the Oh number is 0.00233 in the oval tube with $a = 5$ mm and $b = 4$ mm, and 0.00308 in the oval tube with $a = 3$ mm and $b = 2$ mm. In the first region, the curve of the data are parabolic, and in the second region, the data fit a straight line. In order to observe this trend more intuitively, a dashed line that starts from the height at t_1 is established. After t_2 , the data deviate from the dashed line, because the height is proportional to \sqrt{t} in the third region. In Fig. 11(b), the Oh number is 0.0452 in the oval tube with $a = 5$ mm and $b = 4$ mm, and 0.0308 in the oval tube with $a = 3$ mm and $b = 2$ mm. The region, in which the meniscus height is proportional to t , does not exist any longer. The flow is divided into two regions under this condition.

More comparisons between theoretical and numerical results are shown in Figs. 12(a)–12(c). The line represents theoretical results and

the square sign stands for numerical results. The black lines and square signs represent data of SF 1, the red lines and square signs represent data of SF 2, and the blue lines and square signs represent data of SF 10. The first region lasts for a short time. In order to show flow features in region 1, more numerical data are plotted than in other regions. While in experiments, owing to the wetting barriers obstruction, it is hard to measure the meniscus position at the beginning. So, experimental data start from 0.2 s or 0.3 s. It can be seen that numerical results are all in good agreement with theoretical ones. And, the increase in viscosity will significantly slow down the flow rate.

Figures 13(a)–13(d) show the comparison between theoretical, experimental, and numerical results. In the figures, the curves represent the theoretical height vs time, and the red square signs stand for the numerical results and the black square signs stand for the experimental results. The results of the three methods are in good agreement. The moments that demarcate different regions are also labeled. Figures 13(a) and 13(b) present that, in the first region, the curve of the data are parabolic, and in the second region, the data fit a straight line. And after t_2 , the data deviate from the dashed line. Figures 13(c)

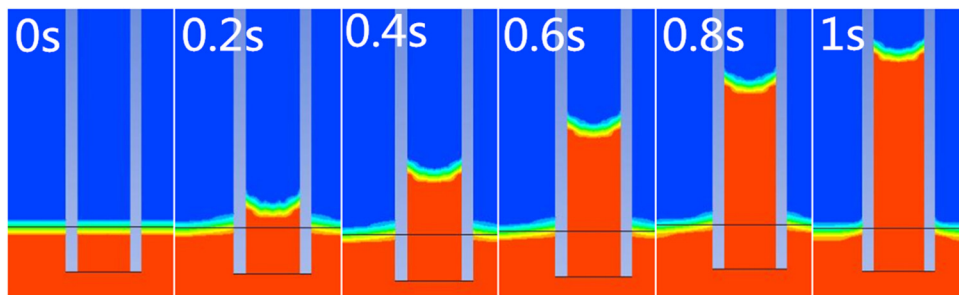


FIG. 10. A vertical cross section of the numerical model. The liquid is SF 2 (12.3 °C) and $a = 7$ mm, $b = 4$ mm, and $h_0 = 12$ mm.

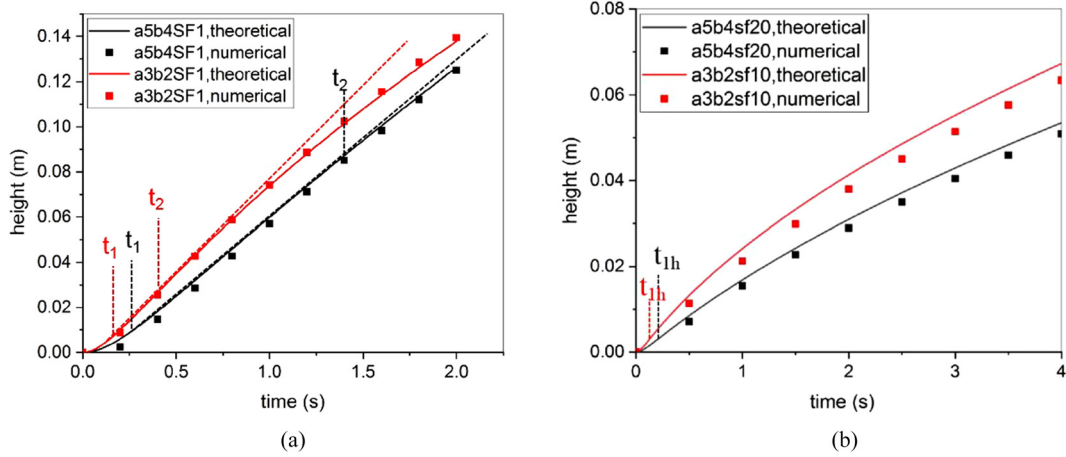


FIG. 11. Comparison between theoretical and numerical results. (a) SF 1 (25 °C) in the oval tube with $a = 5$ mm, $b = 4$ mm, $h_0 = 20$ mm, and SF 1 (25 °C) in the oval tube with $a = 3$ mm, $b = 2$ mm, and $h_0 = 15$ mm. (b) SF 10 (25 °C) in the oval tube with $a = 3$ mm, $b = 2$ mm, $h_0 = 15$ mm, and SF 20 (25 °C) in the oval tube with $a = 5$ mm, $b = 4$ mm, and $h_0 = 20$ mm.

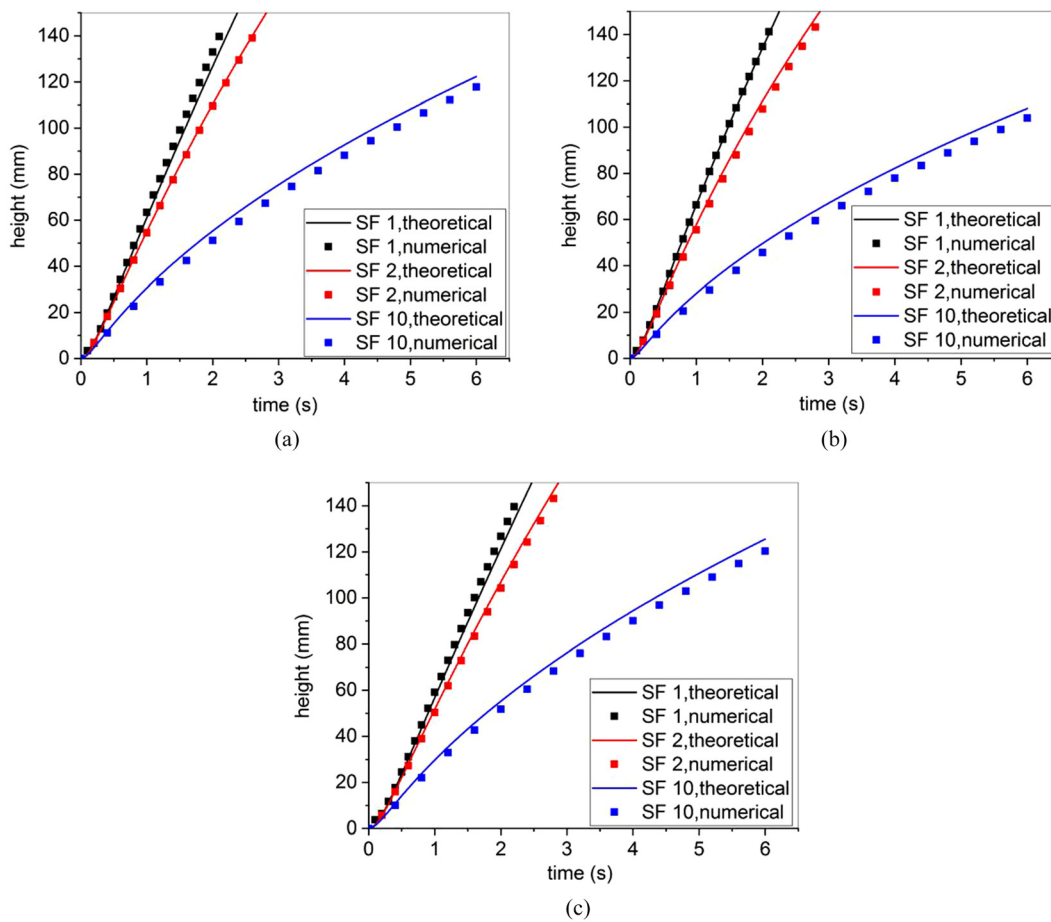


FIG. 12. Comparison between theoretical and numerical results. (a) $a = 7$ mm, $b = 4$ mm, $h_0 = 12$ mm, (b) $a = 6$ mm, $b = 3$ mm, $h_0 = 15$ mm, and (c) $a = 6$ mm, $b = 5$ mm, $h_0 = 15$ mm.

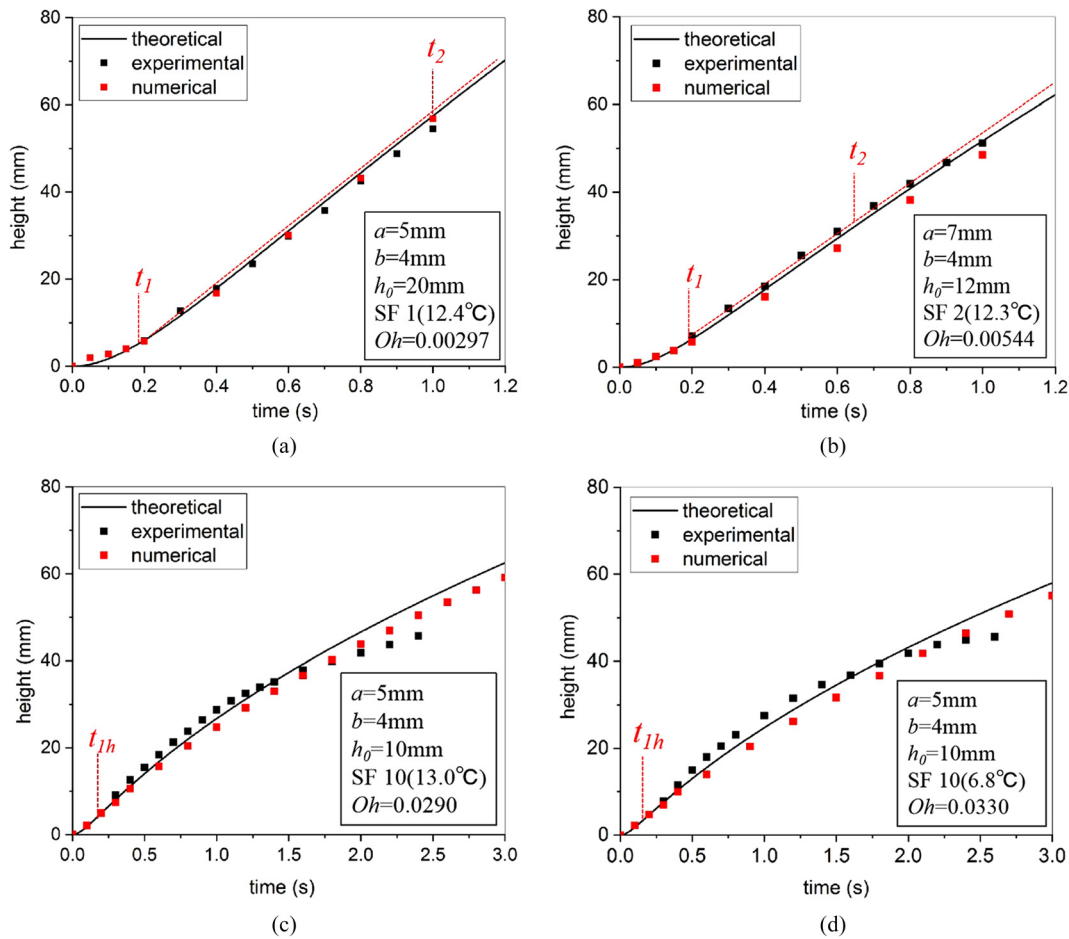


FIG. 13. Comparison between theoretical, experimental, and numerical results. (a) SF 1 (12.4 °C) in the oval tube with $a = 5$ mm, $b = 4$ mm, $h_0 = 20$; (b) SF 2 (12.3 °C) in the oval tube with $a = 7$ mm, $b = 4$ mm, $h_0 = 12$; (c) SF 10 (13.0 °C) in the oval tube with $a = 5$ mm, $b = 4$ mm, $h_0 = 10$; (d) SF 10 (6.8 °C) in the oval tube with $a = 5$ mm, $b = 4$ mm, and $h_0 = 10$.

and 13(d) show that the flow is divided into two regions. All of these features accord with theoretical analysis above. It is a pity that limited by the camera’s field of view, the flow distance is less than 80 mm. And during drop tower experiments, the free surface in the reservoir did not change from flat into a curved one slowly as imagined. Owing to wetting barriers obstruction and vibration caused by release, the free surface in the reservoir kept shaking slightly during experiments and exceeded wetting barriers. This leads to deviation between experimental data and theoretical results in late period in Figs. 13(c) and 13(d). The reservoir will be enlarged and optimized to reduce its impact and more experiments will be carried out.

V. SUMMARY

The exact equation for capillary driven flow into oval tubes is obtained and verified by drop tower experiments and numerical simulation with the VOF method. Several sizes of oval tubes and four kinds of Silicone Fluids are used in our analysis. The theoretical result is in good agreement with the experimental and numerical results.

Moreover, an approximate solution by considering simplified forces is also presented. In the case of low Oh numbers, by using the capillary force as the driving force and balancing it with the inertia force in the reservoir, the convective pressure loss in the reservoir, and the viscous resistance in the tube, respectively, we can see that the flow behavior is divided into three time domains. In region 1, the capillary driven force and the inertia force in the reservoir play the dominant role. However, the inertia force in the reservoir decreases very quickly, therefore, region 1 just stays for a short time. While the flow enters region 2, the pressure loss in the entrance takes the place of inertia force in the reservoir. The pressure loss decreases with time and the friction force in the tube starts to play an important role, and the liquid flow enters region 3. The liquid climbing height is proportional to t^2 , t , and \sqrt{t} in these three domains, respectively. And in the case of high Oh numbers, the pressure loss in the entrance can be ignored compared to the inertia force in the reservoir and the friction force in the tube, therefore, The region, in which the meniscus height is proportional to t , does not exist any longer. The flow is divided into two regions under this condition.

ACKNOWLEDGMENTS

This research was funded by the China Manned Space Engineering Program (Fluid Physics Experimental Rack and the Priority Research Program of Space Station), the Strategic Priority Research Program of Chinese Academy of Sciences (Grant No. XDB23030300), and the Natural Science Foundation Project (Nos. 12032020 and 12072354).

DATA AVAILABILITY

The data that support the findings of this study are available from the corresponding author upon reasonable request.

REFERENCES

- ¹E. W. Washburn, "The dynamics of capillary flow," *Phys. Rev.* **17**, 273–283 (1921).
- ²P. Concus and R. Finn, "On capillary free surfaces in the absence of gravity," *Acta Math.* **132**, 177–198 (1974).
- ³S. Levine, P. Reed, E. J. Watson, and G. Neale, "A theory of the rate of rise of a liquid in a capillary," *Colloid Interface Sci.* **3**, 403–419 (1976).
- ⁴M. Stange, M. Dreyer, and H. Rath, "Capillary driven flow in circular cylindrical tubes," *Phys. Fluids* **15**, 2587–2601 (2003).
- ⁵T.-S. Jiang, S.-G. Oh, and J. C. Slattery, "Correlation for dynamic contact angle," *J. Colloid Interface Sci.* **69**, 74–77 (1979).
- ⁶M. Dreyer, A. Delgado, and H. J. Rath, "Capillary rise of liquid between parallel plates under microgravity," *J. Colloid Interface Sci.* **163**, 158–168 (1994).
- ⁷M. M. Weislogel and S. Lichter, "Capillary flow in an interior corner," *J. Fluid Mech.* **373**, 349–378 (1998).
- ⁸M. M. Weislogel and C. L. Nardin, "Capillary driven flow along interior corners formed by planar walls of varying wettability," *Microgravity Sci. Technol.* **17**(3), 45–55 (2005).
- ⁹Y. K. Chen, M. Weislogel, and C. Nardin, "Capillary driven flows along rounded interior corners," *J. Fluid Mech.* **566**, 235–271 (2006).
- ¹⁰F. J. Higuera, A. Medina, and A. Linan, "Capillary rise of a liquid between two vertical plates making a small angle," *Phys. Fluids* **20**, 102102 (2008).
- ¹¹F. Wolf, L. Santos, and P. Phillippi, "Capillary rise between plates under dynamic conditions," *J. Colloid Interface Sci.* **344**, 171–179 (2010).
- ¹²D. A. Bolleddula, Y. K. Chen, B. Semerjian *et al.*, "Compound capillary flows in complex containers: Drop tower test results," *Microgravity Sci. Technol.* **22**, 475–485 (2010).
- ¹³Y. Q. Li, M. Z. Hu, L. Liu *et al.*, "Study of capillary driven flow in an interior corner of rounded wall under microgravity," *Microgravity Sci. Technol.* **27**, 193–205 (2015).
- ¹⁴E. Reyssat, "Capillary bridges between a plane and a cylindrical wall," *J. Fluid Mech.* **773**, R1 (2015).
- ¹⁵Z. Y. Wu, Y. Y. Huang, X. Q. Chen *et al.*, "Capillary driven flows along curved interior corners," *Int. J. Multiphase Flow* **109**, 14–25 (2018).
- ¹⁶V. R. Dushin, V. F. Nikitin, N. N. Smirnov *et al.*, "Microgravity investigation of capillary driven imbibition," *Microgravity Sci. Technol.* **30**(4), 393–398 (2018).
- ¹⁷R. Chassagne, F. Dörfler, M. Guyenot *et al.*, "Modeling of capillary driven flows in axisymmetric geometries," *Comput. Fluids* **178**, 132–140 (2019).
- ¹⁸C. Shangdong, H. Zhiyi, D. Li *et al.*, "Experimental and numerical study on capillary flow along deflectors in plate surface tension tanks in microgravity environment," *AIP Adv.* **9**, 025020 (2019).